Dislocation Simulation of Brittle-Ductile Transition in Ferritic Steels

S.J. NORONHA and N.M. GHONIEM

Two-dimensional discrete dislocation simulations of the crack-tip plasticity of a macrocrack-microcrack system representing the fracture behavior in ferritic steels are presented. The crack-tip plastic zones are represented as arrays of discrete dislocations emitted from crack-tip sources and equilibrated against the friction stress. The dislocation arrays modify the elastic field of the crack; the resulting field describes the elastoplastic crack field. The simulated crack system involves a microcrack in the plastic zone of the macrocrack (elastoplastic stress field). The effects of the crack-tip blunting of the macrocrack are included in the simulations; as dislocations are emitted, the microcrack is kept at a constant distance from the blunted tip of the macrocrack. The brittle-ductile transition (BDT) curve is obtained by simulating the fracture toughness at various temperatures. A consideration of the effects of blunting is found to be critical in predicting the sharp upturn of the BDT curve. The obtained results are compared with existing experimental data and are found to be in reasonable agreement.

I. INTRODUCTION

IT is now a well-accepted fact that the fracture of ferritic steels in the temperature range in which the fracture propagates by cleavage is originated in microcracks (mostly in precipitates), ahead of the macrocracks; the macrocracks could be either precracks in a test specimen or surface cracks in structures. The extremely high fracture toughness (>20 MPa$\sqrt{m}$, compared with 1 MPa$\sqrt{m}$ calculated from the surface energy alone, assuming the pure cleavage of the Fe matrix) observed at low temperatures in ferritic steels is due to the fact that cleavage is initiated and propagated from microcracks ahead of the macrocracks.[1] It has been found by experiments that these microcracks are originated in precipitates,[2,3] and that the propagation of these microcracks into the matrix is assumed to be the controlling step in the fracture of ferritic steels. Another observation, though less ambiguously established, is that the cleavage stress at fracture on these microcracks is invariant with temperature.[4–8]

Ritchie, Knott, and Rice[9] used both the solutions developed by Hutchinson-Rice and Rosengren and a finite element analysis (FEA) to simulate the plastic zone; a critical tensile stress achieved over a characteristic distance ahead of the crack is used as the failure criterion. This distance is essentially a fitting parameter, and Ritchie, Knott, and Rice used a value equal to or twice the average grain diameter. The model successfully predicts the lower-shelf fracture toughness, but fails to predict the upturn near the transition temperature. Statistical models were introduced to predict the brittle-ductile transition (BDT) in steels, starting with Curry and Knott;[3] most notable among them were by Beremin[10] and Wallin *et al.*[11] In both these models, FEA solutions of crack-tip plasticity were used to obtain the stress fields ahead of the crack. In the Beremin model, the maximum principal stress is calculated for each volume element in the plastic zone and a probability of failure is assigned. The total probability of failure is then obtained by summing over the entire plastic zone. Wallin *et al.* extended the modeling to the transition region by considering the variation in the effective surface energy ($\gamma_s + \gamma_p$) with temperature, where γ_s is the true surface energy and γ_p is the plastic work done during propagation. This eventually led to the master curve (MC) hypothesis, which predicts that the BDT of all ferritic steels follows a universal curve.[11,12] Even though the MC is used to check the reliability of structures under irradiation,[14] a clear understanding of the physical basis of this methodology is still lacking.[15] Odette *et al.*[13] explained the MC using a microscopic fracture stress varying with temperature. Most experimental findings[7,8] indicate that the fracture stress is not sensitive to temperature; more careful experiments and simulations may be required to resolve this issue.

Discrete dislocation simulations of crack tips were successful in predicting the BDT of simple single crystalline materials, for example, in References 16 and 17. The advantage of this approach over the continuum methods is that fundamental material properties such as dislocation velocity and their mutual interactions can be treated dynamically. Through these simulations, it has been found that the dislocation mobility plays a significant role in determining the transition temperature.[17] However, the variation in the dislocation mobility alone cannot explain the BDT behavior. An earlier attempt to model the BDT of complex materials such as steels[18] predicted the lower-shelf fracture toughness, which substantiated Orowan's postulate[1] on high fracture toughness measured at low temperature. However, the model failed in predicting the sharp increase in fracture toughness around the transition temperature region.

Here, we present a discrete dislocation simulation, in which crack-tip blunting is taken into account for the first time. The effects of blunting are incorporated into the simulation by using elastic stress fields of blunted cracks. As the crack tip gets blunted due to the dislocation emission, the position

S.J. NORONHA, Lecturer and Research Associate, and N.M. GHONIEM, UC Distinguished Professor, are with the Department of Mechanical and Aerospace Engineering, University of California, Los Angeles, CA 90095-1597. Contact e-mail: snoronha@ucla.edu

This article is based on a presentation made in the symposium "Computational Aspects of Mechanical Properties of Materials," which occurred at the 2005 TMS Annual Meeting, February 13–17, 2005, in San Francisco, CA, under the auspices of the MPMD–Computational Materials Science & Engineering (Jt. ASM-MSCTS) Committee.

of the "virtual sharp crack tip" retreats from the blunted tip, thereby further reducing both the field at the microcrack and the contribution from the emitted dislocations. The critical particle is assumed to be at a fixed distance from the blunted macrocrack tip.

In Section II, we outline the detailed procedure of the methodology used in the simulation of the crack tip. Section III describes the results obtained in our simulations; we compare our predictions with the experimental results reported in the literature. In Section IV, we summarize our results and discuss the possible implications of our model.

II. MODEL AND METHOD OF CALCULATION

A. *Problem Formulation*

From numerous careful experimental studies conducted on the BDT behavior of steels, it is now established that: (1) precracks (macrocracks) blunt substantially before the fracture of the specimen occurs at the transition region. However, the examination of the fracture surface reveals that cracks propagate predominantly by cleavage;[4] (2) several cracked, brittle particles are found to be present in the broken samples;[5,7] and (3) the measured microscopic fracture stress (at microcracks) is found to be a few orders of magnitude higher than that of the pure Griffith value.[7,8] All these observations are considered in our model, as follows.

(a) We implemented the blunting of the macrocrack by using the elastic crack-tip stress field for blunted cracks. As dislocations are emitted, the crack blunts and the radius of curvature increases. The notional crack tip, which is taken as the reference for the calculation of image stresses, retreats away from the blunted tip.
(b) A microcrack is placed in the field of a macrocrack; the failure criterion used in the calculation is the cleavage crack propagation from this microcrack.
(c) We consider the emission of dislocations and the subsequent shielding from the microcrack tip. (A detailed study of this and of the observed constancy for microscopic fracture stress is reported in an earlier study.[19])

B. *Overview of the Model*

The geometry of the model used for simulation is shown in Figure 1. A semi-infinite crack (macrocrack), with a finite microcrack situated ahead of it on its crack plane, is loaded starting from $K = 0$. Dislocation sources are assumed to exist at distances x_0 from the tip, and are situated on the slip planes passing through the crack tip. During loading, dislocations are emitted from source positions (x_0) when the resolved shear stress reaches a value $2\tau_y$. The resolved shear stresses are obtained using expressions based on derivations for both a semi-infinite crack[23] and a finite crack.[20] The emitted dislocations move along the slip plane away from the crack tip, and the stress at the source increases, until another dislocation is emitted. The emitted dislocations move with a velocity based on the following expression:

$$v_{x_i} = \left(\frac{|\tau_{x_i}| - \tau_y}{\tau_{x_i}}\right)\left(|\tau_{x_i}|\right)^m A e^{(-Ea/kT)} \qquad [1]$$

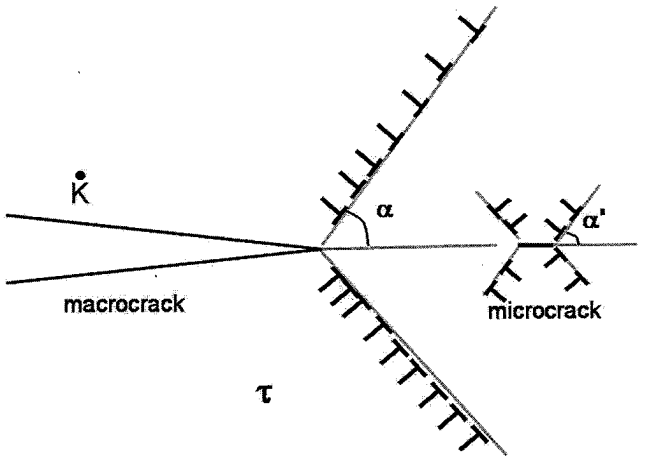

Fig. 1—The geometry of the crack and dislocations used in the macrocrack-microcrack simulation model. The K is the applied load at the macrocrack, the slip plane angles are oriented at α and α' to the crack planes of the macrocrack and microcrack, respectively.

The values for the parameters were obtained by fitting the data related to the screw dislocation velocities in iron.[22] The value of m has a linear dependence on temperature, T, $m = 400/T + 1.2$, $A = 3.14 \times 10^{-4}$ meters s^{-1} $(MPa)^{-m}$, and $E_a = 0.316$ eV. The first term restricts the motion of dislocations below the friction stress value (τ_y), making sure that $v = 0$ for $|\tau_{x_i}| < \tau_y$; hence, most of the dislocations are in near-equilibrium positions at any given time. When the dislocations are in their equilibrium positions, the temperature and the strain-rate dependence of the measured fracture toughness (K_F), plastic zone size (d_F), crack-tip opening displacement, *etc.*, are determined only by the temperature and the strain-rate dependence of the friction stress (τ_y). The friction stress (τ_y) experienced by dislocations is due to the effect of all types of obstacles in dislocation motion, including impurities, precipitates, grain boundaries, *etc.*, in addition to the lattice friction. The τ_y used is chosen to be equal to the shear-yield stress $\sigma_y/2$ when the Tresca yield criterion is assumed; the σ_y corresponds to the measured uniaxial yield stress at a given temperature. The temperature-yield stress relation used throughout this article is obtained from the data reported in Reference 3. Thus, the temperature dependence of the fracture toughness is obtained by inputting the corresponding friction stress value for each temperature. Simulations are done for temperatures ranging from −180 °C to −60 °C, with corresponding yield stresses (σ_y) from 910 to 620 MPa.

The arrays of emitted dislocations form the plastic zones of the crack. The crack may also get blunted, due to dislocation emissions. In our case, the effects of blunting will be negligible for microcracks, since the number of dislocations emitted is only up to 10^2. Whereas the effects of blunting will be significant in the case of macrocracks, because the number of dislocations emitted is of the order 10^5, the blunting effects are accounted for here by using the elastic crack-tip field as a blunted crack.[24] The plastic zone developed at the macrocrack changes the field ahead of it into an elastic-plastic material with hardening.[25] The microcrack placed in this field experiences a tensile stress and is assumed to propagate, which leads to fracture when it reaches a critical value σ_F (estimated based on similar dislocation

simulations of finite crack-emitting dislocations along the slip planes).

As described later, our simulations are done in two stages: (1) the microcrack is loaded to failure and the microscopic fracture stress is estimated for specific crystallographic orientations and crack sizes, and (2) the obtained microscopic fracture stress (σ_F) values are then used as the fracture criterion in the macrocrack simulation.

C. *Method of Calculation*

1. *Simulation of the microcrack*

A microcrack of the configuration shown on the right side of Figure 1 is loaded monotonically. To mimic the triaxial stress field surrounding the microcrack (since it is located in the plastic zone ahead of a macrocrack), we modified the expressions for the stress fields given in Reference 20 by subtracting the applied normal stress (σ_{Ay}) and adding the uniaxial yield stress (σ_y), for cases in which $\sigma_{Ay} > \sigma_y$. (For a detailed discussion, see Reference 19.) The values of the slip plane angle α' are chosen such that predominantly brittle crack configurations are simulated. The applied load is incremented at a rate dK/dt (= 0.01 MPa$\sqrt{\text{ms}^{-1}}$); a variable time-step is used to make sure dislocations move as an array and numerical instabilities are avoided. Dislocations are emitted from source positions (here chosen as $4b$, b = 2.54 Å, following an earlier study on the effect of source position[19]) along the slip planes. Since source positions are equidistant from their respective crack tips, simultaneous emission occurs. The emitted dislocations move away from the crack tip along the slip planes with a velocity calculated using Eq. [1]. The stress fields of these dislocations then shield the crack tip from the external load. Once the emitted dislocations have been moved to their equilibrium positions, the amount of shielding from each dislocation is calculated using expressions from Reference 20, and the total shielding at the crack tip is obtained by summation. We ignore anti-shielding dislocations in our simulations, since any dislocations nucleated in the present configuration around the crack tip will be absorbed by the crack. The number of dislocations thus absorbed is small, and any blunting effects due to the dislocations are neglected here. Since, in our case, dislocations are emitted from crack-tip sources, dislocations emitted from either end contribute to shielding both crack tips.[21] The applied load is increased monotonically and the crack-tip stress intensity is calculated at each time-step. When the crack-tip stress intensity reaches a preassigned critical value, the crack is assumed to propagate and the corresponding applied load is the microscopic fracture stress (σ_F). The following two predominantly brittle microcrack systems are considered here: (1) cleavage plane (001), crack front [110], and slip system $1/2[\bar{1}11](1\bar{1}2)$ (hence α' = 35 deg, 16 minutes), and (2) cleavage plane (110), crack front $[\bar{1}10]$, and slip system $1/2[111](11\bar{2})$ (hence α' = 54 deg, 44 minutes).

2. *Simulation of the macrocrack*

A schematic illustration of the macrocrack is shown on the left-hand side of Figure 1. The macrocrack is assumed to be semi-infinite, with dislocation sources close to the crack tip. Dislocations are emitted simultaneously along the two slip planes, and are symmetrically oriented to the crack plane. The plastic zone formed by the emitted dislocations produces a field equivalent to an elastic-plastic crack with small-scale yielding.[25] The agreement with continuum models has substantially improved, compared to previous estimations from asymmetric single-slip plane cases, as, for example, in Reference 18. The slip-plane angle, in this case, is chosen to be 70.5 deg (the direction of maximum shear stress of the elastic crack-tip field); compared to other slip-plane angles, this value matches best with continuum estimates.[25] The initial source position (x_0) along the slip plane is chosen to be $4b$, where b is the magnitude of Burgers vector.

During the simulation, the applied stress intensity is increased in small increments and the positions of dislocations are determined. As the load is increased, more and more dislocations are emitted and the crack gets blunted. The radius of the blunted crack ρ is taken to be equal to N b sin α, where N is the number of dislocations and α is the slip-plane angle. The blunting of the macrocrack is illustrated in Figure 2. As blunting increases: (1) the crack-tip fields are modified to be that of a blunted crack,[24] (2) the source position is chosen to be equal to the crack-tip radius, *i.e.*, $x_0 = \rho$, and (3) the notional crack tip from which the image stress of dislocations is calculated is moved back to the center of the curvature of the blunted crack. At each time-step, the stress ahead of the crack at a distance X_p along the crack plane (the microcrack is assumed to be at this position) is calculated using the expression from Reference 23. The fracture criterion is the tensile stress (σ_{yy}^{p}) at X_p reaching σ_F, calculated in the previous stage for the microcracks for the same temperature and for the corresponding yield stress. Thus, when the microcrack-tip stress intensity, $k = K_{Ic}$, cleavage fracture of the matrix is assumed to occur. The applied load at the macrocrack then gives the fracture toughness (K_F) at that given temperature and yield stress. Throughout the simulation, a microcrack 1 μm in size is used; this value is chosen as a typical (average) value in the range of the sizes of the microcracks found in experiments with which we compare our results.[3] The detailed simulations reported here are obtained using Xp equal to 10 μm. However, the K_F calculated using 20 μm is also shown in Figure 6. These values were chosen as typical values of the order of the grain sizes in these types of steels. It should be noted that changing

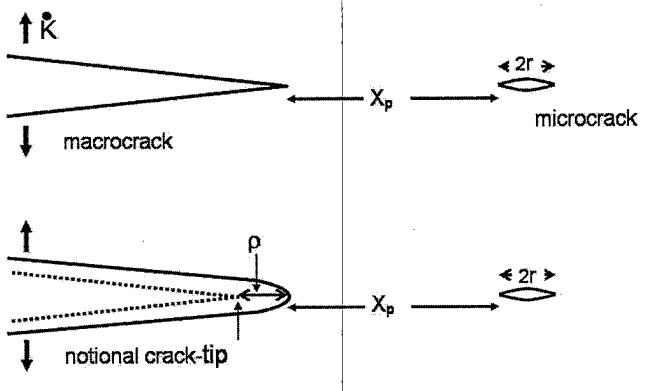

Fig. 2—Schematic illustration of the crack-tip blunting. The ρ is the radius of the blunted crack tip, $2r$ is the microcrack size, and X_p is the distance of the microcrack from the macrocrack tip. The distance of the microcrack from the notional sharp crack tip increases from X_p to $X_p + \rho$.

these parameters will give different values for the fracture toughness; however, the form of their variation with temperature will remain the same, as will be discussed in Section III.

III. RESULTS AND DISCUSSION

A. *Microcrack Simulation: Calculation of Microscopic Fracture Stress (σ_F)*

Figure 3 shows the results from the microcrack simulation: dislocation sources emitting dislocations along four symmetric slip planes around the through-thickness crack shown in Figure 1. The (micro) fracture stress σ_F, as a function of temperature, is shown for two different slip-plane angles, $\alpha' = 35$ deg, 16 minutes and 54 deg, 44 minutes, corresponding to the crack system (001) [110] with slip system $1/2[\bar{1}11](1\bar{1}2)$, and (110) [110] with slip system $1/2[111](11\bar{2})$, respectively. The fracture criterion chosen was the crack-tip stress intensity $k = K_{Ic} = 1.0$ MPa$\sqrt{\text{m}}$ (the value estimated for *Fe* with a surface energy of 2 Jm^{-2}). The microscopic fracture stress, σ_F, is estimated for different temperatures; it can be seen that the fracture stress σ_F is practically independent of temperature, consistent with many of the experiments, as shown, for example, in Reference 7. Similar results were reported earlier in Reference 19. The value of σ_F thus obtained for each temperature is used to calculate the macroscopic fracture toughness (K_F) in the next stage of the simulation, described here.

B. *Macrocrack Simulation: Calculation of Fracture Toughness (K_F)*

Figure 4 shows a typical behavior of the tensile stress at the microcrack ($\sigma_{yy}{}^p$) as a function of the applied load (K). The fracture criterion in this case is $\sigma_{yy}{}^p$, which reaches the critical value σ_F, which was calculated in the previous stage. For the case shown here, the size of the microcrack is 1 μm; the rate of loading is $dK/dt = 0.01$ MPa$\sqrt{\text{m}}$s^{-1}. As the temperature is increased and the yield stress (friction stress) is decreased, the applied stress intensity K required for the tensile stress at X_P to reach the critical value σ_F increases exponentially. Two possible factors contributing to this exponential increase are the decrease in the tensile stress at the microcrack due to the crack-tip blunting and the increasing effects of the stress field (predominantly compressive) from the emitted dislocations. This can be seen in Figure 4(b), where the plastic zone size (d_F) and the radius of the blunted crack tip (ρ_F) for each temperature measured at fracture, K-applied $= K_F$ is shown. The plastic zone size is the distance measured along the slip plane of the farthest dislocation from the crack tip. The dislocation source distance (x_0) is chosen as ρ for a crack-tip radius greater than $4b$; otherwise, $x_0 = 4b$. Figure 5(a) shows the macroscopic fracture toughness, K_F, as a function of temperature, for cases with and without considering the effects of crack-tip blunting. For the case without blunting, the increase in the fracture toughness (K_F) with temperature is small; on the other hand, a sharper increase in the fracture toughness is observed when blunting is accounted for in the simulation. This striking observation emphasizes the significant effect of blunting in the increase of fracture toughness with temperature. This exponential increase in the fracture toughness corresponds to the transition from brittle to ductile behavior.

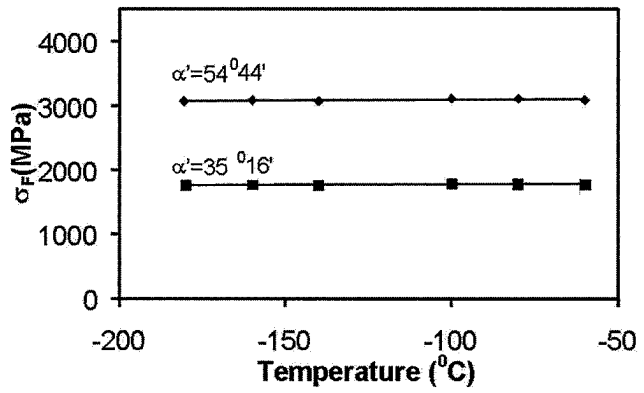

Fig. 3—The microscopic fracture stress (at the microcrack tip) as a function of temperature; the crack size = 1 μm.

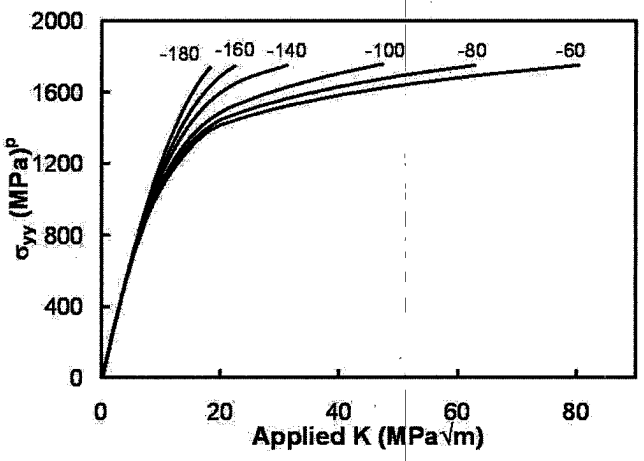

(*a*)

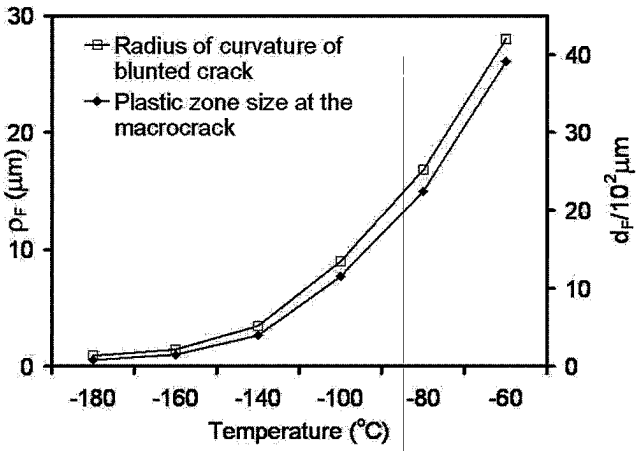

(*b*)

Fig. 4—(*a*) The tensile stress at the microcrack ($\sigma_{yy}{}^p$) as a function of the (K_{app}) or the simulation time for different yield stresses. The corresponding temperatures in degrees centigrade are shown in the plot and (*b*) the crack-tip radius (ρ_F) and the plastic zone size (d_F) calculated at K_F for each temperature are shown.

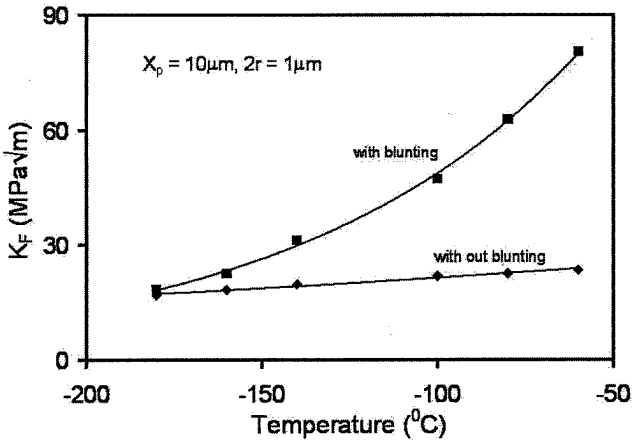

(*a*)

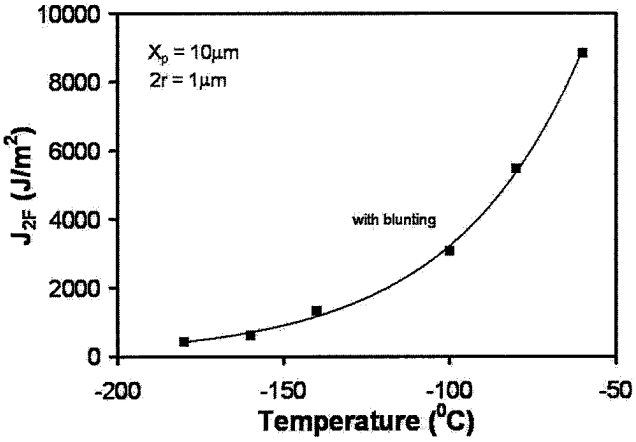

(*b*)

Fig. 5—(*a*) The fracture toughness (K_F) as a function of temperature, for cases with and without blunting; the microcrack size = 1 μm and (*b*) the J_{2F-} integral calculated for the different temperatures for the blunting case shown in Figure 5(a).

In Figure 5(b), the J_{2F}, the J_{2-} integral value at fracture, calculated from the number of dislocations emitted at the corresponding load K_F, is shown. The J_2 is defined as the sum of the glide forces on all dislocations around the crack tip.[26] In this case, the dislocations are in equilibrium against the friction stress (τ_y), and we can compute J_{2F} as the product of the total number of dislocations (N) and the friction stress (τ_y). Considering the fact that J_{2F} is calculated from the number of dislocations emitted at an applied stress intensity factor, K_F, it is striking to note that the prefactor of the exponent of the J_{2F-} temperature curve (0.0255) matches with that of the K_{F-} temperature curve (0.0123), to hold the known proportionality between K^2 and J.

In Figure 6, the calculated values of fracture toughness are compared with the fracture toughness measurements reported in Reference 3. The carbide sizes found in these samples range in size from 0.44 to 1.32 μm; in our calculations, we have used microcracks of comparable size (1 μm). The results for the blunted case, shown in Figure 5(a) along with a set of values calculated with X_P = 20 μm, is shown here for comparison. We can see that the model predicts the rapid increase in fracture toughness at the transition temperature region, and reasonably fits the experimental data.

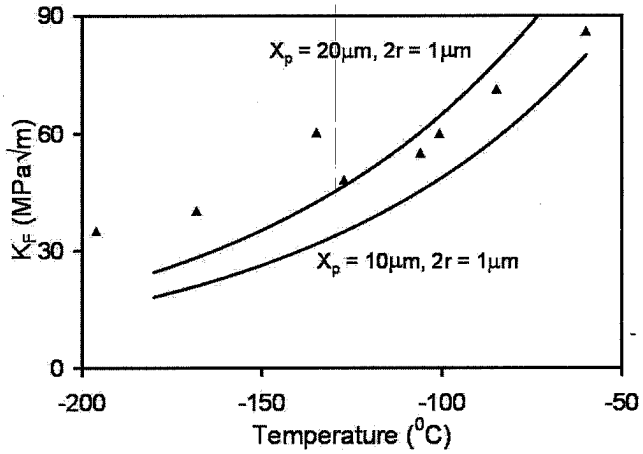

Fig. 6—The fracture toughness values from Figure 5(a) (X_p = 10 μm) and for X_p = 20 μm are compared with experimentally determined values.[3]

Considering the simplicity of the present model, the agreement is a good step in predicting the BDT behavior.

IV. SUMMARY AND CONCLUSIONS

A two-dimensional dislocation dynamics simulation is used to study the crack system involved in the fracture of ferritic steels; this involves a macrocrack with microcracks ahead of it. The crack-tip behavior and the BDT predicted have good agreement at the transition region, where the fracture toughness increases rapidly with temperature. However, it should be noted that the model ceases to be valid at higher temperatures, at which ductile tearing effects will be significant. According to our model, the two factors that contribute to the sharp increase in the fracture toughness with temperature are: (1) the increase in the mobility of the emitted dislocations and (2) the effect of the crack-tip blunting of the macrocrack. The mobility of emitted dislocations determines the equilibrium position of the dislocations and, thus, also determines the tensile stress at the microcrack. Additionally, the mobility of the dislocations around the microcrack determines the crack-tip stress intensity at the microcrack and, thus, the microscopic fracture toughness (σ_F), which itself ultimately determines the fracture toughness of the material (K_F). However, as can be seen in Figure 5(a), this alone cannot explain the sharp upturn at the transition. The amount of crack-tip blunting is found to be a significant factor in capturing the rapid increase in the fracture toughness with temperature in the transition region.

REFERENCES

1. E. Orowan: *Trans. Inst. Eng. Shipbuilders Scotland*, 1945, vol. 89, p. 165.
2. C.J. McMahon, Jr. and M. Cohen: *Acta Metall.*, 1965, vol. 13, p. 591.
3. D.A. Curry and J.F. Knott: *Met. Sci.*, 1979, vol. 13, p. 341.
4. P. Bowen and J.F. Knott: *Metall. Trans. A*, 1986, vol. 17A, p. 231.
5. M.K. Veistinen and V.K. Lindroos: *Scripta Metall.*, 1984, vol. 18, p. 185.
6. P. Bowen, S.G. Druce, and J.F. Knott: *Acta Metall.*, 1986, vol. 34, p. 1121.
7. P. Bowen, S.G. Druce, and J.F. Knott: *Acta Metall.*, 1987, vol. 35, p. 1735.

8. S.R. Ortner and C.A. Hippsley: *Mater. Sci. Technol.*, 1996, vol. 12, p. 1035.
9. R.O. Ritchie, J.F. Knott, and J.R. Rice: *J. Mech. Phys. Solids*, 1973, vol. 21, p. 395.
10. F.M. Beremin: *Metall. Trans. A*, 1983, vol. 14A, p. 2277.
11. K. Wallin, T. Saario, and K. Törrönen: *Met. Sci.*, 1984, vol. 18, p. 13.
12. D.E. McCabe, J.G. Merkle, and K. Wallin: in *Fatigue and Fracture Mechanics: 30th Volume*, ASTM STP 1360, P.C. Paris and K.L. Jerina, eds., ASTM, West Conshohocken, PA, 2000, p. 21.
13. G.R. Odette and M.Y. He: *J. Nucl. Mater.*, 2000, vols. 283–287, p. 120.
14. ASTM Standard Test Method E 1921–02, *Annual Book of ASTM Standards*, ASTM, West Conshohocken, PA, 2002, vol. 03.01.
15. M.E. Natishan and M.T. Kirk: in *Fatigue and Fracture Mechanics: 30th Volume*, ASTM STP 1360, P.C. Paris and K.L. Jerina, eds., ASTM, West Conshohocken, PA, 2000, p. 51.
16. P.B. Hirsch, S.G. Roberts, and J. Samuels: *Proc. R. Soc. London A*, 1989, vol. 421, p. 25.
17. P.B. Hirsch and S.G. Roberts: *Phil. Mag. A*, 1991, vol. 64, p. 55.
18. P.B. Hirsch and S.G. Roberts: *Phil. Trans. R. Soc. London A*, 1997, vol. 355, p. 1991.
19. S.G. Roberts, S.J. Noronha, A.J. Wilkinson, and P.B. Hirsch: *Acta Mater.*, 2002, vol. 50, p. 1229.
20. S. Wang and S. Lee: *Mater. Sci. Eng.*, 1990, vol. A130, p. 1.
21. T-Y. Zhang and J.C.M. Li: *Acta Metall. Mater.*, 1991, vol. 39, p. 2739.
22. H. Saka, K. Nada, and T. Imura: *Crystal Lattice Defects*, 1973, vol. 4, p. 45.
23. V. Lakshmanan and J.C.M. Li: *Mater. Sci. Eng.*, 1988, vol. A104, p. 95.
24. M. Creager and P.C. Paris: *Int. J. Fract. Mech.*, 1967, vol. 3, p. 247.
25. S.J. Noronha and N.M. Ghoniem: unpublished research.
26. M.X. Shi, Y. Huang, and H. Gao: *Int. J. Plasticity*, 2004, vol. 20, p. 1739.